An Ultrasound Application for TiO₂ Photocatalytic Degradation of Methyl Orange

Xianzhen DIAO *, Jing XU, Yufei WANG

Chemistry and Chemical Engineering College, Chongqing Institute of Science and Technology, Chongqing, 401331, China

Nanometer TiO_2 photocatalysts were prepared by the sol–gel method. The catalysts were characterized by X-ray diffraction, Fourier-transform infrared spectroscopy, ultraviolet-visible spectroscopy, and other techniques. Methyl orange solution was used for the degradation of the organic material and ultrasonic technology was used to determine the photocatalytic performance of the catalysts. The results show that the photocatalytic performance of the Ni-N-TiO_2 is clearly improved under ultrasonic conditions. The TiO_2 photocatalytic degradation effect is optimal at a catalyst concentration of 0.3 g/L, an initial concentration of the organic matter of 0.03 mmol/L, a nickel-doping amount of 2 mol %, and a nitrogen-doping amount of 15 mol %. The use of ultrasound technology in combination with photocatalysis has a positive effect and results in a TiO_2 degradation rate of methyl orange of 95 % after 3 h.
Keywords: TiO_2, photocatalysis, ultrasound.

1. INTRODUCTION

Photocatalytic technology has many advantages for the treatment of polluted air and wastewater and represents an important development regarding environmental protection. Titanium dioxide (TiO_2) is widely applied in the field of photocatalysis due to its physical and chemical properties of stability, high catalytic activity, and low cost, among many other advantages. However, due to the forbidden bandwidth, TiO_2 can only absorb ultraviolet light, restricting the practical applications of TiO_2. Solar energy is a relatively new and renewable energy source and may represent the most important energy source in the near future because of increasingly scarce resources and increasing consumption. The ultraviolet range represents less than 5 % of the entire light spectrum and the sunlight utilization of TiO_2 during photocatalysis is quite insufficient, which has become current photocatalyst to overcome difficulties [1 – 3].

The unique ultrasound cavitation effect has been applied for wastewater treatment [4]. Recent developments have included the combination of various processing technologies, such as ultrasonic catalytic oxidation, a combination of ultrasonic radiation, and other oxidation techniques. The intense turbulence caused by ultrasonic radiation strengthens the solid-liquid mass transfer between the organic pollutants and the solid catalyst, which cleans the surface of the catalyst, maintains the catalyst's activity, and improves the degradation efficiency [5]. Studies have shown that ultrasonic-photocatalytic techniques improved to the treatment of organic wastewater [6 – 12].

In this study, nanometer TiO_2 photocatalysts were used with ultrasound technology for the treatment of organic wastewater; modifications of the catalysts and photocatalytic degradation effects were explored. The optimum conditions were determined by the characterization of the catalysts and performance degradation experiments were conducted. It is expected that this study can provide production test values for the practical application of ultrasonic photocatalysis.

2. EXPERIMENTAL PROCEDURE

2.1. Preparation methods

Nanometer TiO_2 photocatalysts were prepared by the sol-gel method. At room temperature, 40 ml anhydrous ethanol was poured into a 100 ml beaker, and 20 ml butyl titanate was slowly added under the action of a magnetic stirrer; the mixture was stirred to dissolve the components and obtain solution A. Ten milliliters of distilled water and 14 ml of glacial acetic acid were added to 40 ml of anhydrous ethanol, followed by mixing and slow stirring to obtain solution B. Under vigorous stirring, solution B was poured into solution A. A uniform and transparent sol system appeared after stirring for approximately 1 h; subsequently, the sol was sealed and remained for 24 h, after which a milky jelly-like gel was obtained. The gel was placed in a drying oven at 100 °C for several hours, after which a pale yellow dry gel was obtained. The material was ground and fired for 2 h in a muffle furnace at high temperature, obtaining the nanometer TiO_2 photocatalysts.

A certain amount of nickel nitrate was dissolved in 10 ml of distilled water and was slowly added to a mix of 40 ml anhydrous ethanol and 14 ml glacial acetic acid. The Ni-doped was abtained as the same method. The nickel nitrate of the N-doped and Ni-N-co-doped titanium dioxide was replaced with a urea aqueous solution and a nickel

---

* Corresponding author. Tel.: 13629767386.
E-mail address: *xianzhen81@126.com* (X. Diao)

nitrate solution respectively. The remaining steps were the same as described above.

2.2. Characterization and photocatalytic performance analysis

The crystal structure of nanometer titanium dioxide was analyzed by XRD-7000 X ray diffractometer. The functional groups and bonds existed in the molecules were analyzed using Tensor-27 infrared spectrometer $(400-4000 \text{ cm}^{-1})$.

A 30-W UV lamp was used as the light source and a methyl orange solution was used as the target of degradation. The initial concentration of the methyl orange solution with a *pH* of 6 was 0.01 mmol/L. Using a 250 ml beaker, 0.03 g of the catalyst was added to 100 ml of the methyl orange solution. The mixture was kept in the dark and was mixed for 30 min to achieve the adsorption equilibrium in solution. The solution was then placed under the UV lamp for photocatalytic degradation and the solution (or ultrasonic cleaning machine) was stirred at 20 min sampling intervals for the first hour and at 30 min sampling intervals after two hours. Subsequently, the absorbance was measured and changes in the performance were determined.

3. RESULTS AND DISCUSSION

3.1. X-ray diffraction spectrum analysis

Fig. 1 and Fig. 2 show the X-ray diffraction (XRD) spectra of pure TiO_2 for different calcination temperatures. It has been reported [13] that the diffraction angles 2θ 25.37°, 37.03°, 37.88°, 38.61°, 48.12°, 53.97°, 55.1 0°, 62.14°, and 68.79° belong to the crystal plane diffraction peaks of the anatase phase (101), (103), (004), (112), (200), (105), (211), (213), (204), (116), (220), and (215) respectively; the diffraction angles 2θ 27.48°, 36.12°, 39.24°, 41.28°, 44.08°, 54.36°, 56.68°, 62.80°, 64.12°, 69.04°, and 69.80° correspond to the diffraction peaks of the rutile phase (110), (101), (200), (111), (210), (211), (220), (002), (310), (301), and (112) respectively.

Fig. 1 shows that the TiO_2 diffraction peak intensity increases with an increase in the calcination temperature and that the width of the diffraction peak narrows. At a treatment temperature of 400 °C, the peak of the TiO_2 is not obvious because the grain growth is not complete. At a calcination temperature of 500 °C, the TiO_2 has an anatase phase structure. At a temperature of 600 °C, the characteristic peaks of the anatase phase are reduced and the characteristic peaks of the rutile phase increase, indicating the existence of anatase and rutile phases. When the temperature reaches 700 °C, the anatase phase of the TiO_2 is almost completely transformed into the rutile phase.

Fig. 2 shows that the rutile phase of the doped TiO_2 appears at 700 °C, indicating that nickel and nitrogen doping inhibit the shift of the anatase phase to the rutile phase. Fig. 1 and Fig. 2 show that, at the same temperature, the diffraction peaks are wider for the doped TiO_2 than for the pure TiO_2. The Scherrer formula is defined as:

$$D=K\lambda/\beta_{1/2}cos\theta, \tag{1}$$

where *d* is the particle size, *K* is Scherrer constant (approximately 0.89 when using Cu target), λ is the wavelength of X ray, θ is the diffraction angle, β is the half-peak width of the main peak, in radians.
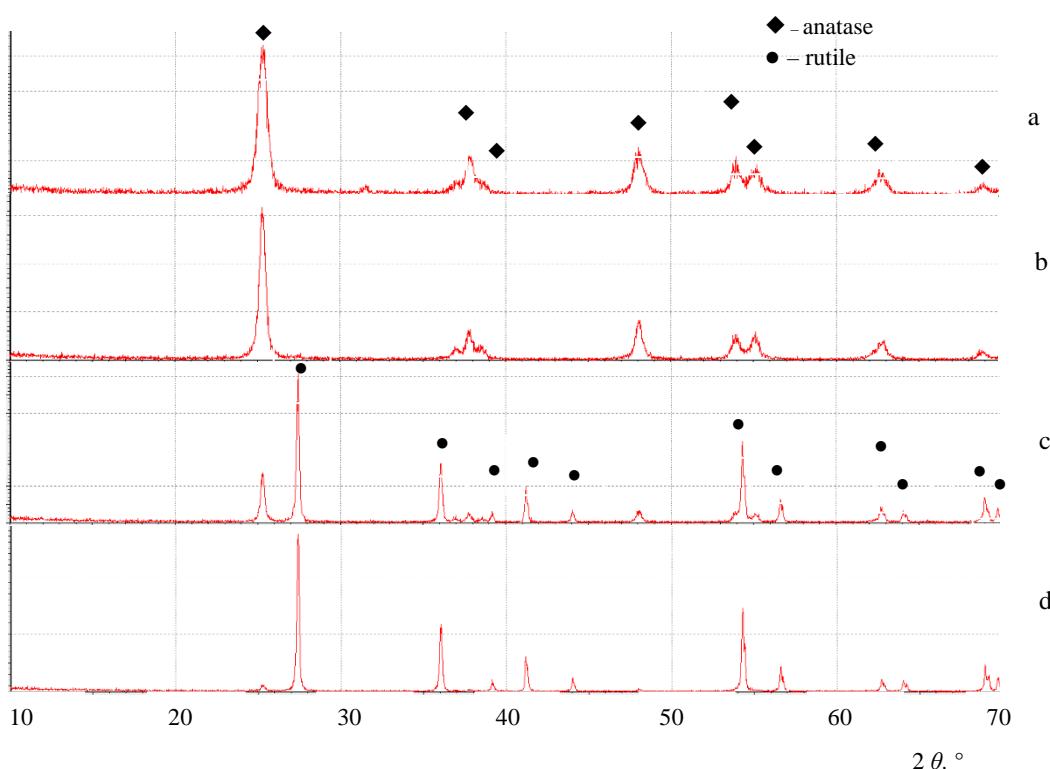
Fig. 1. XRD spectra for pure TiO_2 for different calcination temperatures: a – 400 °C; b – 500 °C; c – 600 °C; d – 700 °C
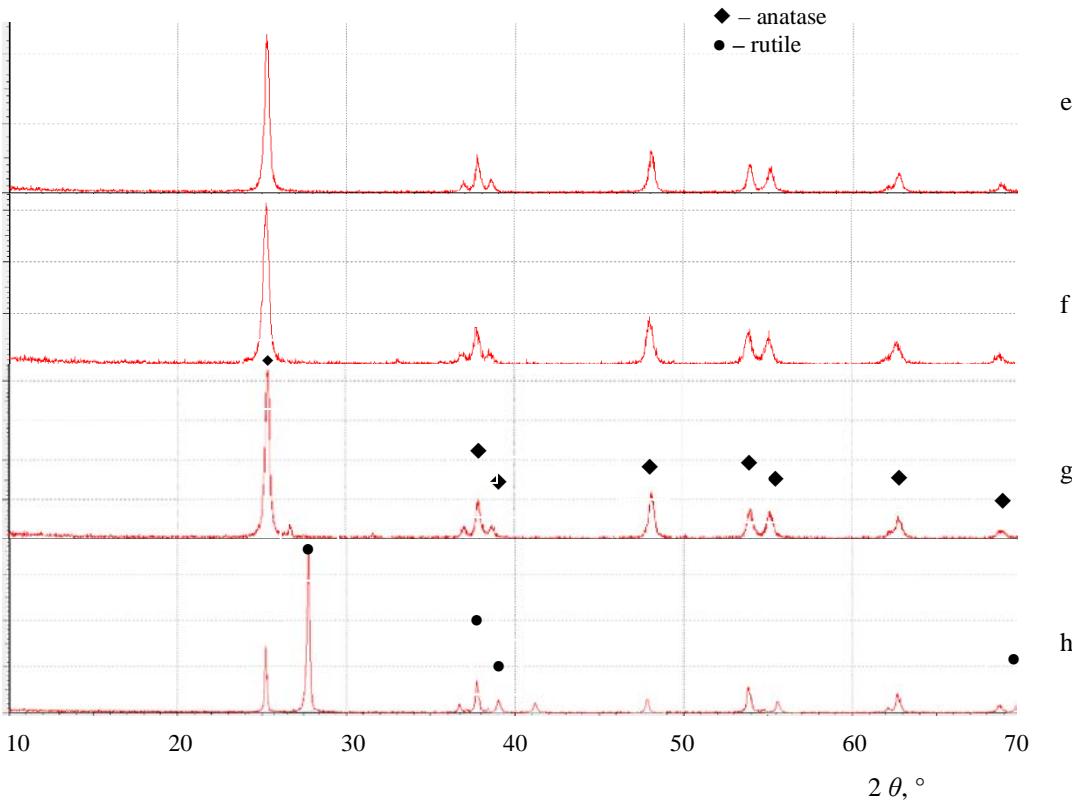
Fig. 2. XRD spectra for doped TiO₂ for different calcination temperatures: a – 15 mol % N-TiO₂ at 600 °C; b – 2 mol % Ni-TiO₂ at 600 °C; c – 2 mol % Ni- 15 mol % N -TiO₂ at 600 °C; d – 15 mol % N- TiO₂ at 700 °C

The particle size of the pure TiO₂ at 500 °C is 88 nm. At 600 °C, the particle sizes of the N-doped TiO₂, the Ni-N-co-doped TiO₂, and the pure TiO₂ are 66 nm, 67 nm, and 71 nm respectively. The results indicate that an increase in the calcination temperature is beneficial for the growth of the grain and the anatase phase of TiO₂ is gradually transformed into the rutile phase. At 500 °C, the pure TiO₂ is in the anatase phase and as the temperature continues to increase, the rutile phase becomes predominant. At 700 °C, nearly all of the anatase phase TiO₂ has been transformed into the rutile phase. The doped TiO₂ remains in the anatase phase at 600 °C and at 700 °C and the anatase and rutile phase crystal structures coexist. This indicates that nickel and nitrogen doping inhibit a crystal phase shift and result in a decrease in the crystal grain size, which improves the catalytic activity of TiO₂.

3.2. Infrared spectrum analysis

Fig. 3 shows that vibration peaks occurred in the samples at 507 cm⁻¹, 1630 cm⁻¹, 1400 cm⁻¹, 3400 cm⁻¹, and 2400 cm⁻¹. It has been reported that the peak at 1630 cm⁻¹ represents the adsorption of water molecules to the titanium surface or the O-H bond bending vibration; the peak at 3400 cm⁻¹ is the stretching vibration of the water molecules. It is found that the peaks are more pronounced for the doped samples, which indicates that the adsorption of water molecules to the surface of the doped catalyst increases [14]. The peaks at 507 cm⁻¹, 2400 cm⁻¹, and 1400 cm⁻¹ are the Ti-O bond vibration peaks [15], 3341 cm⁻¹ is the -NH₂ peak [16], and 470 cm⁻¹ is the Ti-O-Ni bond contraction vibration absorption peak [17].

The spectrograms show that a larger number of peaks are present in the doped TiO₂, indicating a new functional group. The peak at 3100 cm⁻¹ may be the O-H bond stretching vibration peak (Fig. 3 b). At 2900 cm⁻¹, the C-H bond telescopic absorption peak is observed, which may be attributed to the use of urea as a doping source [18]. The larger number of peaks for the doped TiO₂ is attributed to the doping elements as well as the presence of impurity peaks due to the butyl titanate ester hydrolysis.

3.3. UV-Vis spectrum analysis

Fig. 4 shows the ultraviolet-visible (UV-Vis) absorption spectra of different TiO₂ photocatalysts. The absorption sidebands of pure TiO₂, 15 mol % N-TiO₂, 2 mol % Ni-TiO₂, and 2 mol % Ni 15 mol % N-TiO₂ are 387 nm, 400 nm, 420 nm, and 400 nm respectively. The band-gap energy is calculated using the formula:

$$E = hc / \lambda; \qquad\qquad (2)$$

where h is Planck's constant; c is the speed of light; λ is the cutoff wavelength ($h = 6.626 \times 10^{-34}$, $c = 3.0 \times 10^8$, $1 eV = 1.6 \times 10^{-19}$ J). The band-gap energy values are 3.2 eV for pure TiO₂ , 3.1 eV for 15 mol % N-TiO₂, 2.9 eV for 2 mol % Ni-TiO₂, and 3.1 eV for 2 mol % Ni 15 mol % N-TiO₂. The absorbance increases at first and then decreases. The doped TiO₂ catalysts have wider absorption sidebands and stronger light intensities than the pure TiO₂. This may be because the non-metallic Ni, N doping results in an impurity level between the conduction band and the valence band of TiO₂, effectively narrowing the band gap and improving the responsiveness to visible light.
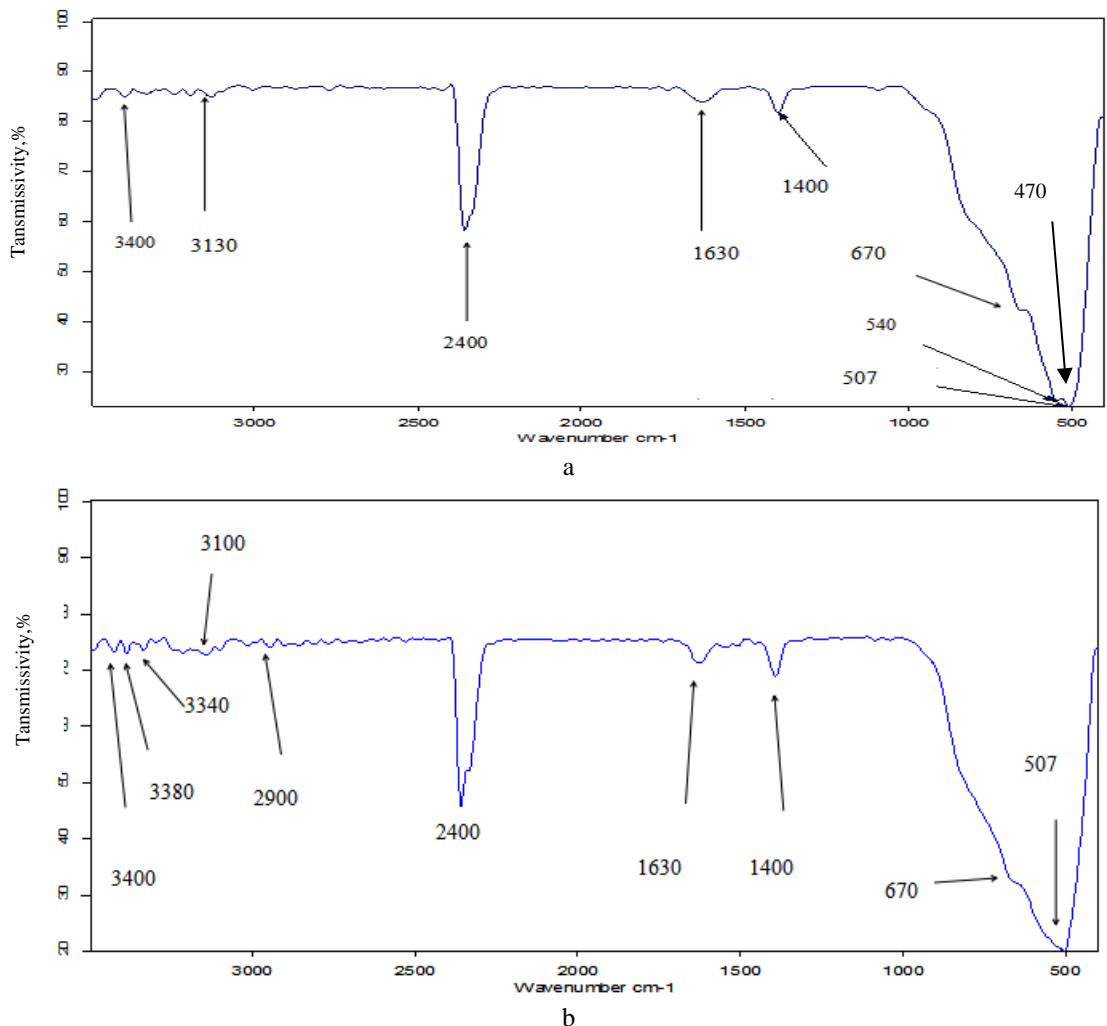
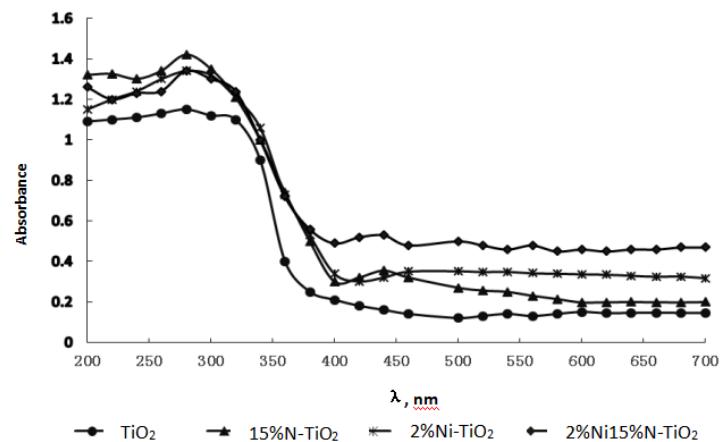**Fig. 3.** TiO$_2$ transmission spectra: a – TiO$_2$; b – Ni-N-TiO$_2$

Fig. 4. Absorption spectra of TiO$_2$ catalysts doped with different materials

3.4. TiO$_2$ photocatalytic performance

3.4.1. Influences of doping amounts

Fig. 5 shows that the amount of Ni doping amount has an influence on the catalytic activity of TiO$_2$. At a Ni molar content of 2 %, the photocatalytic efficiency is the highest at 81 %. Earlier research has shown that metal ions are introduced inside the crystal lattice and this impurity causes lattice defects [19]. On the one hand, the excitation wavelength of light is extended to the visible light; on the other hand, the formation of lattice defects serves as a trap for light carriers and inhibits the improvement in the catalytic activity by the light carriers. When the amount of doping material is small, the ions entering the crystal lattice do not cause lattice defects and the crystal structure cannot reach the optimal state; therefore, the TiO$_2$ does not achieve an optimum value of light catalysis. When the amount of doping material is excessive, leading to active carrier

258

compound due to defects as new recombination center and the catalytic activity of the TiO₂ is affected. Excessive ion doping affects the crystal structure of the TiO₂ and the catalytic performance is affected to a certain degree. The results indicate that an increase in the doping amount of the catalyst results in an increase followed by a decrease in the degradation efficiency; this is in agreement with the theory [20].
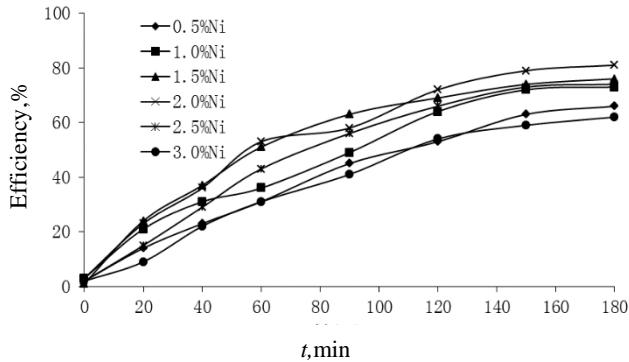

Fig. 5. TiO₂ degradation rates for different amounts of nickel doping

Fig. 6 shows that the degradation rate is highest for the 15 mol % N-TiO₂ and reaches 79 %. Research has shown that non-metallic elements partly replace the oxygen in the oxygen–titanium bond, that hybridizes orbit, forming a new level, changing the forbidden band level, narrowing the width, and thus widening the wavelength range of the light response, thereby improving the photocatalytic activity. When the amount of doping material is very low, the optimum state of the energy level cannot be achieved and the capture trap is ineffective. When the amount of doping material is excessive, as the temperature rises, the nitrogen overflows or the crystal surface structure changes and the photocatalytic activity of TiO₂ is affected.
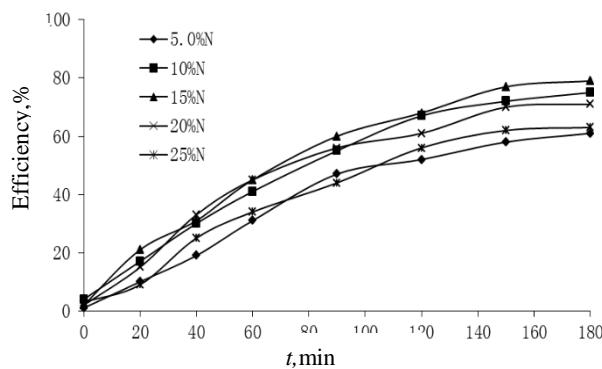

Fig. 6. TiO₂ degradation rates for different amounts of nitrogen doping

3.4.2. Ultrasonic-TiO₂ photocatalytic degradation results

Fig. 7 shows that the degradation effect was higher for the doped TiO₂ than for the pure TiO₂ and reached 80 % after 3 h. The degradation rate is slightly higher for the Ni-N-co-doped TiO₂ than for the N-doped and Ni-doped products. The degradation rate is lowest for the pure TiO₂ at only 63 %. Fig. 8 shows that the degradation rate of the TiO₂ photocatalyst was higher for the ultrasonic photocatalysis and reached 95 % after 3 h.
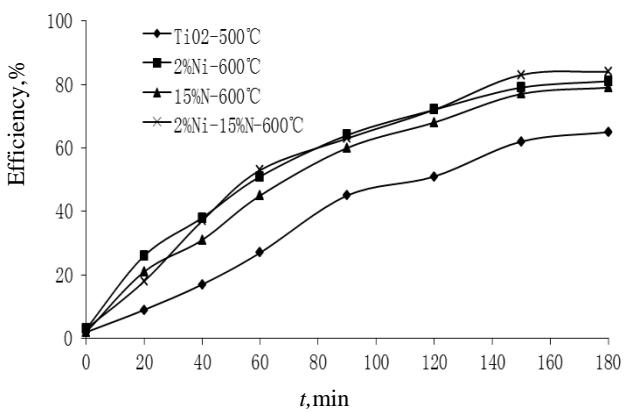

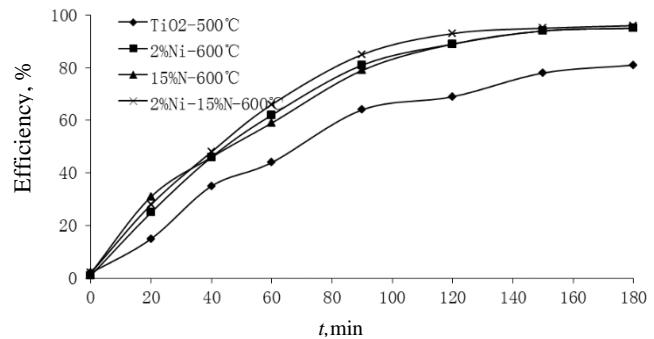**Fig. 7.** Photocatalytic degradation effects of different catalysts

Fig. 8. Ultrasonic photocatalytic degradation effects of different catalysts

A comparison of the data shown in Fig. 7 and Fig. 8 indicates that TiO₂ has an improved effect on the degradation of methyl orange when using ultrasonic-assisted photocatalysis(rated power at 400W and frequency at 40KHz). The degradation rates increase over time within 2 h and stabilize after 2 h, indicating that to some extent, the combination of ultrasound and light catalytic degradation results in improvements. The reason may be as follows: ultrasonic oxidation and TiO₂ photocatalysis oxidation represent advanced oxidation technologies. On the one hand, the ultrasonic cavitation effect produces hydroxyl free radicals under high temperature and high pressure and is capable of degrading products that TiO₂ cannot degrade. TiO₂ is also able to degrade intermediate products that cannot be degraded by ultrasound. Therefore, the effect of the combined technologies is improved and results in improved organic oxidation. On the other hand, the ultrasonic technology has a mechanical dispersion effect that prevents the accumulation of the catalyst and accelerates the heat and mass transfer of the degradation system; as a result, the utilization rate of the catalytic surface is improved.

4. CONCLUSIONS

Nickel-doped TiO₂, nitrogen-doped TiO₂, and nickel and nitrogen co-doped TiO₂ were prepared by the sol-gel method. Nickel nitrate was used as the nickel source and urea was used as the nitrogen source. The catalysts were characterized by XRD, FT-IR, and UV-Vis. A methyl orange solution was used for the degradation of the organic material and ultrasonic technology was used to determine

the factors affecting the photocatalytic activity of TiO_2 through performance degradation experiments. The experimental results showed that the photocatalytic performance of the nickel and nitrogen co-doped TiO_2 is improved using the ultrasonic technology. The TiO_2 photocatalytic degradation effect is optimal at a catalyst concentration of 0.3 g/L, an initial concentration of the degradation liquid of 0.03 mmol/L, a nickel-doping amount of 2 %, and a nitrogen-doping amount of 15 %. When the ultrasound and photocatalysis methods are combined, the TiO_2 degradation rate of methyl orange is 95 % after 3 h, which is higher than the results of 80 % when only photocatalysis is used. Through the research, it is hoped that ultrasonic- photocatalysis can provide practical reference value in environmental governance.

REFERENCES

1. **Wu, Y.L., Jin, H., Li, Y.** Preparation and Photocatalytic Properties of Many Branch of TiO_2 Nanoparticle Arrays.New *Chemical Materials* 43 (4) 2015: pp. 152 – 154.

2. **Sun, P., Zhang, G.Q.** Preparation of 13X Zeolite/TiO_2 Composite Photocatalyst and Photocatalytic Degradation of Methylene Blue *Green IT* 10 2016: 238 – 239. https://doi.org/10.16663/j.cnki.lskj.2016.10.090

3. **Zhang, X.J., Deng, B.Y.** Liu QS. Preparation and Properties of ACF Loaded N Doped TiO_2 Photocatalyst *New Chemical Materials* 44 (6) 2016: pp. 138 – 140.

4. **Wang, H.J., Chen, J.Y**. Ultrasonic-Fe^{3+} Doped TiO_2 Nanotube Photocatalytic Degradation of Reactive Brilliant Red x-3b *Nanomaterials and Applications* 9 (1) 2012: pp. 14 – 17.

5. **Zhang, X.J., Li, S.Q., Deng, B.Y.** Preparation and Performance Study of TiO_2/ACF Photocatalytic Materials *Applied Chemical Industry* 44 (12) 2015: pp. 2239 – 2242. https://doi.org/10.16581/j.cnki.issn1671-3206.2015.12.019

6. **Deng, Y., He, Q.Q.** Research Progress and Application of TiO_2 Photocatalytic Materials *Guangzhou Chemical Industry* 44 (17) 2016: 55 – 56.

7. **Zhong, X.L., Han, X.X., Ruan, W.D., Yang, X.W.** Study on Enhancement of Raman Scattering PATP on the Surface of Ag/TiO_2 Nanotube Base and Photocatalytic Process *Spectroscopy and Spectral Analysis* 36 (6) 2016: pp. 1740 – 1744. https://doi.org/10.3964/j.issn.1000-0593(2016)06-1740-05

8. **He, S.L., Shen, B., Yi, Q., Chen, J.Y.** Study on the Photocatalysis of Reactive Black KN-B by Ultrasonic Collaborative TiO_2 *Chinese Ceramics* 51 (6) 2015: pp. 6 – 9. https://doi.org/10.16521/j.cnki.issn.1001-9642.2015.06.002

9. **Dai, X.J., Tao, H.Y., Zhang, Z.L.** Degradation of Oxytetracycline in Water by Ultrasound and Photocatalysis *Journal of Environmental Hygiene* 7 (2) 2017: pp. 146 – 151. https://doi.org/10.13421/j.cnki.hjwsxzz.2017.02.013

10. **Zhang, Z.L., Liu, Y.F., Niu, J.** Research Progress of Advanced Oxidation Technologies used in the Treatment of Antibiotic Wastewater *Coal and Chemical Industry* 40 (1) 2017: pp. 37 – 39.

11. **Li, H.D.** Full Spectrum Catalysis and Ultrasonic Enhancement Mechanism of Ti-O-based Composite Photocatalyst. Shandong University. 2017.

12. **Liang, W.T., Tian, P., Zhang, H.B.** Study on the Treatment of Dye Wastewater *Shandong Chemical Industry* 46 2017: pp. 152 – 155. https://doi.org/10.19319/j.cnki. issn.1008-021x.2017.04.064

13. **Ruan, X.C., Wang, W.J., Ai, R.** The Preparation of Ni Doping TiO_2 Photocatalyst and Study on the Catalytic Performance of Anthraquinone Dye Simulated Wastewater *Environmental Science and Technology* 11 (35) 2012: pp. 60 – 64.

14. **Jiang, S.Y., Xu, H.L., Jia, X.H., Lu, L.**Study on Preparation and Photocatalytic Properties of Montmorillonite/TiO_2 Composites *Chemical Mineral and Processing* 3 2012: pp. 15 – 18.

15. **Song, J.X., Zhou, T.L., Ding, J.X.** Study on the Properties of Rare Earth - zeolite-TiO_2 Ternary System Photocatalytic Materials *Journal of Chinese Rare Earth Society* 25 (2) 2007: pp. 172 – 177.

16. **Huang, T, Zhang, G.L., Wang, L., Liu, L.J.** Preparation of Nitrogen Modified Titanium Dioxide by Urea and its Modification Mechanism *Journal of Catalysis* 3 (23) 2011: pp. 508 – 512.

17. **Liu, S.Y., Wu, L.D., Zhao, Z.X.**The Low Thermal Solid Phase Synthesis of Ni-TiO_2 Mesoporous Materials and the Kinetics of Photodegradation of Methyl Orange *Journal of Inorganic Materials* 5 2009: pp. 902 – 908.

18. **Gao, K.** Preparation and Photocatalytic Performance Research of Iron and Nitrogen Doping Nano Titanium Dioxide [Dissertation]. China: Chongqing University of Industry and Commerce; 2009.

19. **Thomas, J., Chitra, K.R.** Nanogold Doped TiO_2 Nanotubes: Efficient Solar Photocatalyst for the Degradation of Endosulfan *Materials Focus* 3 2014: pp. 233 – 238.

20. **Wang, J., Wang, L., He, S.L.** Effect of photocatalytic reduction of carbon dioxide by Mg-Zr Co-doped Nano TiO_2 *Applied Chemical Industry* 2019 (Network starting). https://doi.org/10.16581/j.cnki.issn1671-3206.20190919.015